SOME DIAGNOSTICS OF THE CLOUD/RADIATION INTERACTION IN ECMWF FORECASTING MODEL

J.-F. Geleyn

ECMWF

1. INTRODUCTION

The parameterization of radiation and cloud/radiation interaction in a medium range forecasting model is, technically, not very different from the parallel problem for climate studies with a general circulation model. However once the basic features of the scheme have been designed and tested and one comes to the diagnostic and tuning parts of the development, the emphasis is different. While there is no difficulty in designing sensitivity experiments for the climate model in which changes of the radiation - or cloud/radiation scheme will have a clear influence on the results, the same is not true for 4 to 10 day forecasting; mainly due to the relatively long time scales of radiative-dynamical interactions the effect of reasonable changes in the parameterization scheme are either difficult to detect or cannot be interpreted fully by means of "conventional" diagnostic tools (synoptic maps, skill scores, energy diagrams...). There are four ways out of this difficulty. The first is to extend the period of integration with the same model; we shall not deal here with this possibility since it is expensive and perhaps irrelevant. The second is to exaggerate the changes so that the model's response becomes larger; this may be considered as a first step, necessary before deciding whether or not a given problem is worth investigating; one such example will be mentioned in the next Section. Finally the two more natural, but also more difficult, methods are to design special diagnostic tools for one radiation sensitivity experiment and to design several experiments to focus on one given question; these are the approaches we shall discuss in the latter part of this paper (after describing the ECMWF cloud/radiation scheme) as we primarily are trying to answer the following question: is it worth having an interactive cloud/radiation scheme such as ECMWF's.

2. ONE SET OF "EXTREME" EXPERIMENTS

These experiments were undertaken one year ago at GARP WGNE's request to determine whether or not ECMWF's forecasting model is sensitive to the cloud input to the radiation scheme. Using a case with high predictability (forecasts from 15.2.76) four 10-day integrations were conducted. These were:

A control run (see Section 3 for explanations about the ECMWF system)

B as A but at every radiation computation (12 h apart) cloud cover and liquid water content were zonally averaged after being computed as in A and the averaged values were used in all points for the radiation computation

C as A but every radiation computation used the same cloud field (the one taken from the 10th day of A) without any spatial averaging

D as A but the liquid water content of clouds was multiplied by five, thus giving new optical properties to the clouds.

These experiments attempted to study with brute force methods the sensitivity of the system to: the latitudinal variability of clouds (B/A), the interactive character of cloud patterns with synoptic situations (C/A) and the definition of optical cloud properties (D/A). This "high predictability case" was chosen deliberately, since the departure of runs B, C and D from A is likely to occur at a late stage of the integration. High predictability was the only way to get a preliminary (and partial) answer to the question: when differences appear, which run is best?

The results are summarized in Tables 1 and 2. Table 1 gives the minimum (during the 10-day forecast) correlation of anomalies of geopotential heights between run A and runs B C D for the domain $20^{o}N$ - $82.5^{o}N$/200 mb - 1000 mb. Whenever this minimum is less than 0.5 the time (in days) at which the 0.5 line was first crossed is indicated in brackets (approximate time at which both runs can be considered different from a synoptic point of view. Results are given for the zonal part of the flow, for wave number groups 1-3, 4-9 and 10-20 and for the total flow. Table 2 gives the same values but this time each run is compared to the NMC analysis and the time of the 0.5 crossing represents an estimate of the predictability limit for this case.

Table 1. Northern hemisphere extra-tropical tropospheric anomaly correlations (minimum for 0-10 day forecast period) between the control run (A) and the sensitivity experiments (B, C, D). When appropriate the time (in days) of the first crossing of the 0.5 limit is given.

	zonal	1-3	4-9	10-20	Total
A/B	0.916	0.808	0.681	0.309 (9.4)	0.767
A/C	0.939	0.790	0.319 (7.9)	0.000 (6.7)	0.711
A/D	0.931	0.812	0.611	0.170 (7.5)	0.710

Table 2. Northern hemisphere extra-tropical tropospheric anomaly correlations (minimum for 0-10 day forecast period) between the four runs (A, B, C, D) and the NMC analysis. When appropriate the time (in days) of the first crossing of the 0.5 limit is given

	zonal	1-3	4-9	10-20	Total
A	0.441 (9.6)	0.678	-0.296 (4.5)	-0.106 (2.0)	0.554
B	0.362 (8.6)	0.484 (8.9)	-0.246 (4.6)	-0.066 (2.0)	0.458 (9.8)
C	0.430 (9.7)	0.549	-0.114 (4.6)	-0.172 (2.0)	0.458 (9.8)
D	0.018 (9.0)	0.583	-0.160 (4.5)	-0.137 (2.0)	0.387 (9.2)

These tables indicate - that there is a sensitivity to cloud/radiation parameterization for these experiments, essentially in the non-zonal part of the flow and particularly for the higher wave numbers,

- that the most sensitive of the three aspects tested here is the interaction between clouds and radiation, the least sensitive being their longitudinal distribution (this picture is reversed for the zonal flow),

- that, for this simple case study, the control run (interactive in space and time and with reasonable optical properties for clouds) is the "best run",

- that the more beneficial aspect from this skill score point of view is the longitudinal variability,

- and that in this study sensitivity and positive impact are apparently uncorrelated.

The extreme nature of the test and the use of a single case make all results suspicious, except this one: one cannot simplify the cloud scheme to the extreme without modifying significantly the results of a 10-day integration. In this experiment the superiority of the control run might be due either to chance or to the choice of a high predictability case. However, we felt it interesting to look at the model's energetic to try and find out where this superiority is most evident. The kinetic energy distribution of the long waves (1-3) and the meridional transport of sensible heat by medium waves (4-9) (shown in Fig. 1) are the energetic terms for which the quality of the simulation is directly related to the skill scores.

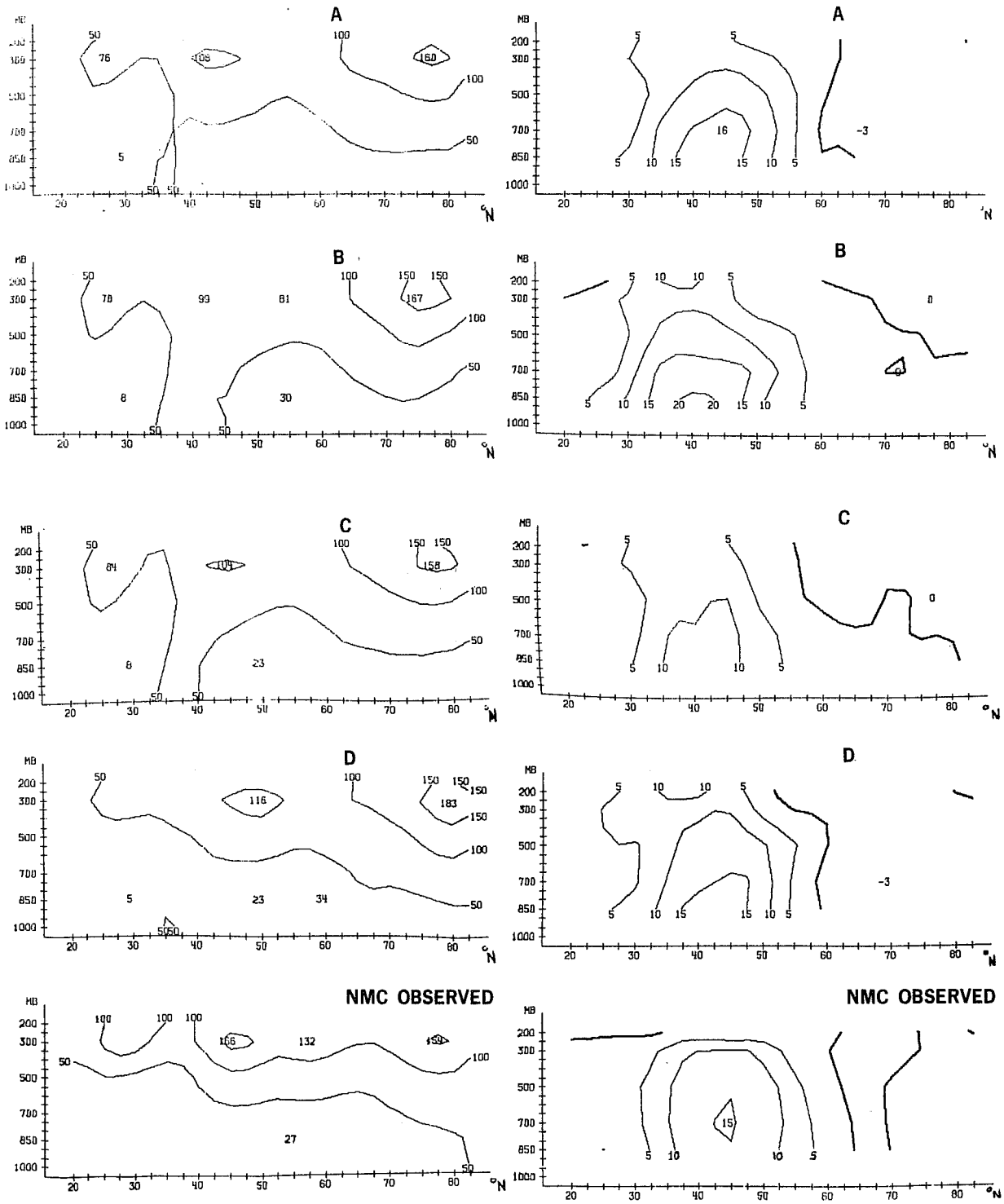

Fig. 1 Latitude/height cross sections for kinetic energy in wavenumbers 1-3 and meridional sensible heat flux in wavenumbers 4-9 for the second half of experiments A, B, C and D and for the observed atmosphere.

3. THE TREATMENT OF THE CLOUD/RADIATION INTERACTION IN ECMWF's MODEL

In this part we shall distinguish between the diagnosis of clouds from prognostic variables of the global model and the influence of these clouds on the computation of radiative fluxes.

For the diagnosis in ECMWF scheme, the clouds used for radiation computations are not directly related to latent heat release (large scale or convective). An attempt to link both radiative and condensation aspects of cloud parameterization was surprisingly not as successful as what will be described now.

The model allows partial or total cloud cover in all its fifteen layers. For each layer a critical relative humidity $RH_C(\sigma)$ has been defined as a function of the vertical coordinate (σ = pressure/surface pressure) alone. Prior to the required calculations the model's relative humidity RH is smoothed along the vertical with a three points filter to become $\overline{RH}$. Then it is compared with $RH_C(\sigma)$. If it is smaller "no cloud" is assumed. If not, for $\overline{RH}$ varying from $RH_C(\sigma)$ to 1 the cloud cover C varies quadratically from 0 to 1 with derivative 0 at $RH_C(\sigma)$ (see Fig. 2A). The functional form for C is therefore:

$$C = \max^2 \left(0, \frac{\overline{RH} - RH_C(\sigma)}{1 - RH_C(\sigma)}\right) \qquad (1)$$

Furthermore in the well mixed boundary layer (potential temperature lower than the surface's one at the considered layer and all layers underneath) we assume C = 0.

The optical properties are evaluated from the cloud's liquid water content taken as a certain fraction $R_{\ell/v}(\sigma)$ of the saturation water vapour content in the cloud; since clouds fully occupy their model layers and have therefore exaggerated depths the above mentioned ratio should be chosen smaller than observed ones. No distinction is made between water and ice clouds.

When tuning this scheme it was decided to keep the number of parameters to a minimum and with no dependence on latitude or time. It was decided that $RH_C(\sigma)$ should be a polynomial of degree 3. Thus, with the two natural conditions $RH_C(0) = RH_C(1) = 1$ we were left with two parameters α and β. Furthermore $R_{\ell/v}$ should be constant in the vertical and equal to the last parameter γ.

$$RH_C = 1 - \alpha\sigma\,(1-\sigma)\,(1+\beta(\sigma - \tfrac{1}{2})) \qquad (2)$$

$$R_{\ell/v} = \gamma$$

The selection of $\alpha\beta$ and γ was completed with the following in mind: to approximate closely the satellite observed profiles of total cloudiness and net radiation as a function of latitude (source: Hoyt (1976)) and to reproduce as well as possible the estimated globally averaged vertical distributions of cloud cover and radiative cooling (sources: London (1952) and Dopplick (1972) combined with Cox and Griffith (1970) as described in the other paper of Cubasch (1981) for this workshop). The choice was $\alpha=2$ $\beta=\sqrt{3}$ $\gamma=0.002$. See Fig. 2B for the profile of $RH_c(\sigma)$.

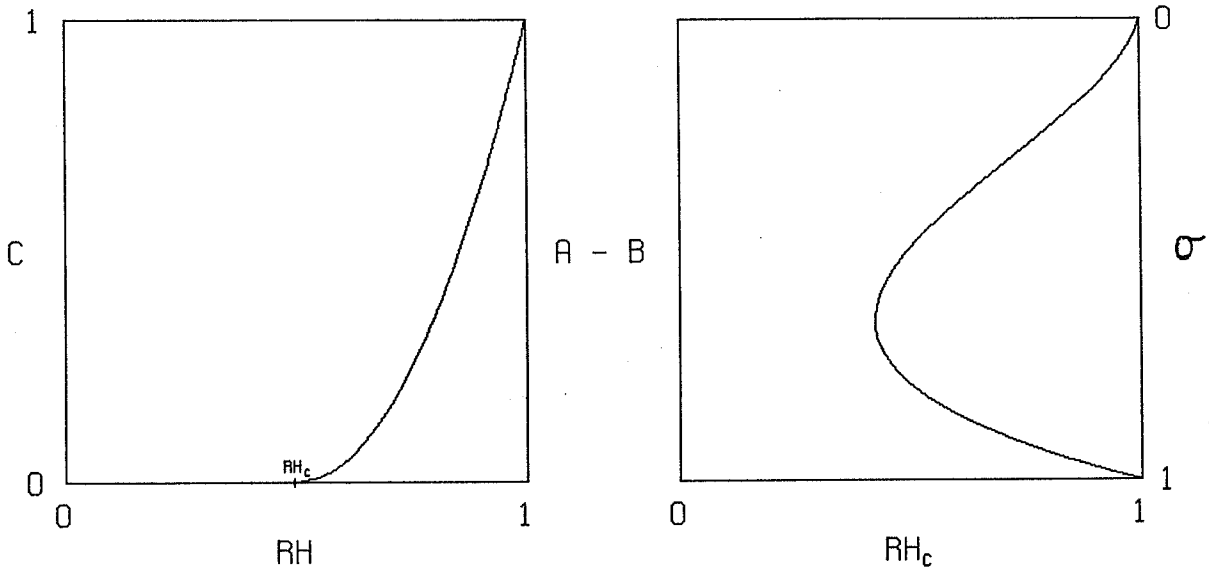

Fig. 2 A: Example of cloud cover as function of relative humidity for a critical value of 0.5 - B: Critical relative humidity as a function of the vertical coordinate σ

The results of our selection can be seen in Fig. 3 where ECMWF operational results for five 10-day forecasts of April 1980 (3rd, 9th, 11th, 21st, 27th) are compared with the above sources (the tuning was done on other cases). Fig. 3A indicates that we have too little cloud cover in the subtropics and this can be interpreted (see for instance Fig. 5) as a failure (at other latitudes as well) to simulate shallow cumuliform clouds. The systematic underestimation of the radiative cooling in 3B can be explained because our global model has a tendency to give a net cooling of the atmosphere by about 1 degree in 10 days and thus the reduced temperature can account for a reduced radiative cooling. However, there is then a relative overestimation in the tropical radiative cooling associated with relatively small surface fluxes in the same areas as seen in 3C. This indicates too low clouds in the tropics. The reason for this deficiency could be the inability of our "relative humidity type" scheme to account for deep convection, or the failure of the convective scheme (in connection with the moisture diffusion scheme) to produce sufficient moistening outside the boundary layer.

Comments about 3D and 3E could be misleading since the confidence in the "observed" values is low. However, the stratospheric cooling and the lack of boundary layer cooling are certainly severe deficiencies of our radiation scheme.

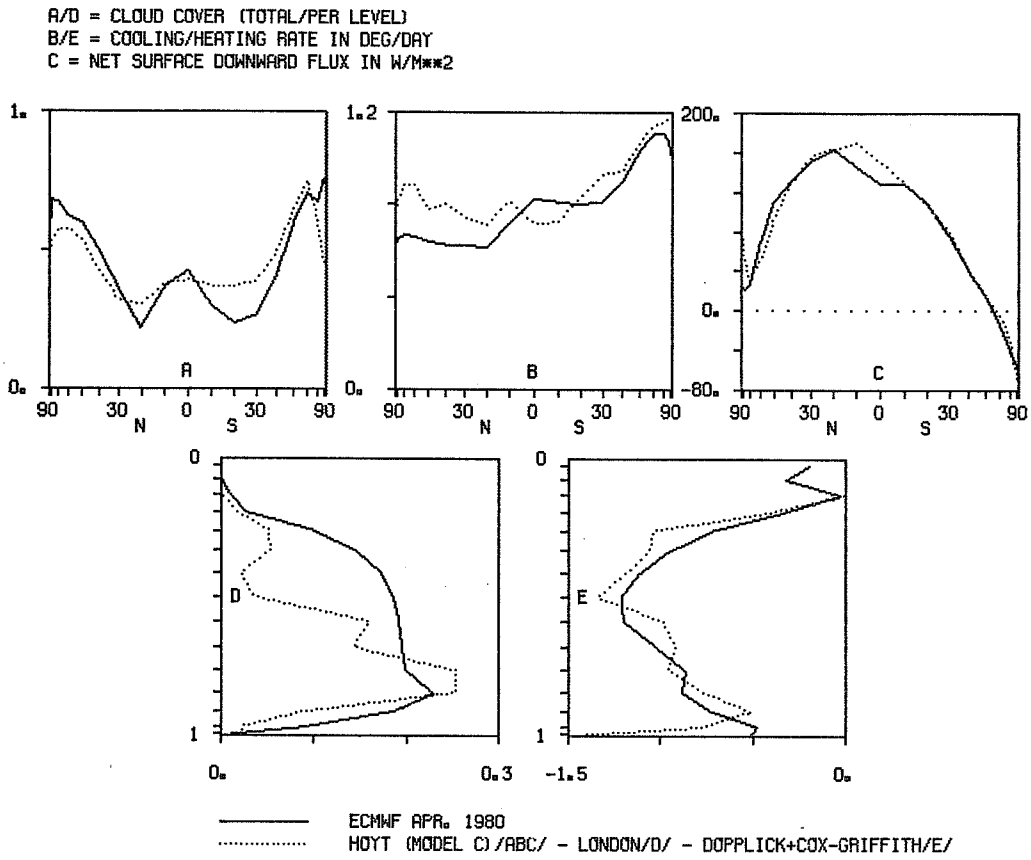

Fig. 3 Comparison (ECMWF results (average over five 10-day operational forecasts)/"observations") for zonal averages of total cloud cover (A), radiative cooling in deg/day (B) and net surface flux in W/m^2 (C) and for global averages of cloud cover (D) and radiative cooling in deg/day (E)

A more detailed description of the cloud structures obtained is given in Fig. 4, where latitude/height cross sections of zonally and time (0-10 day) averaged cloud cover are given for the two integrations with the ECMWF radiation scheme in the set of experiments described for this workshop by Cubasch. These experiments will from now on be labelled by C.F. for the 15.2.76 case and by C.A. for the 25.8.75 case. Seasonal displacements of the main area of clouds are quite realistic but the absence of high tropical clouds is striking.

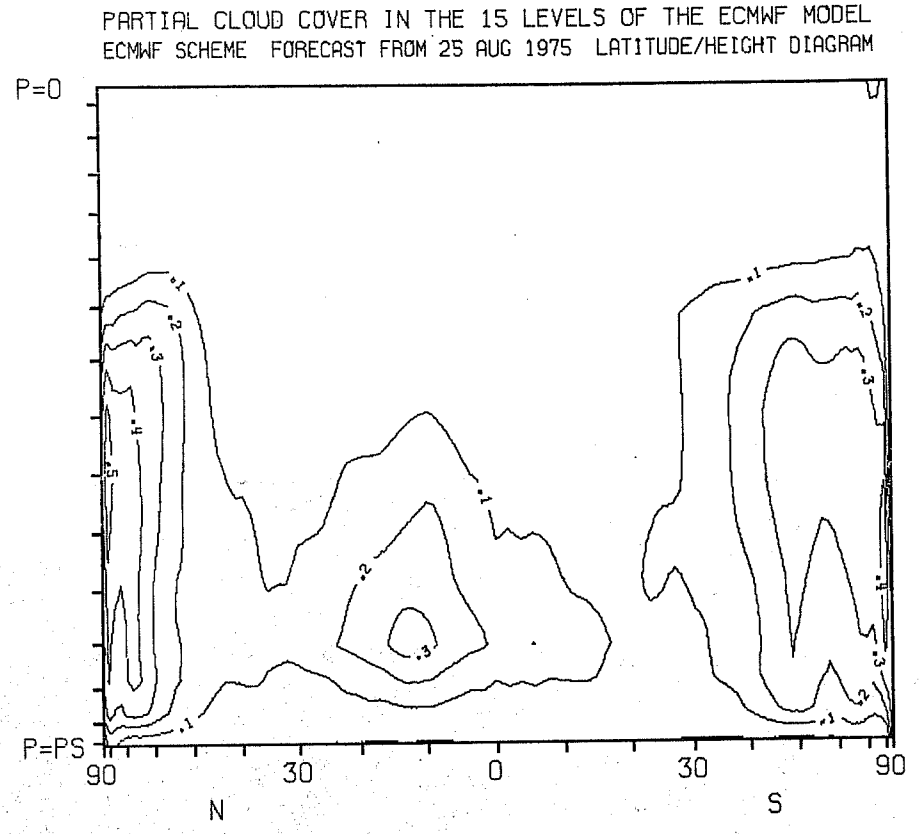

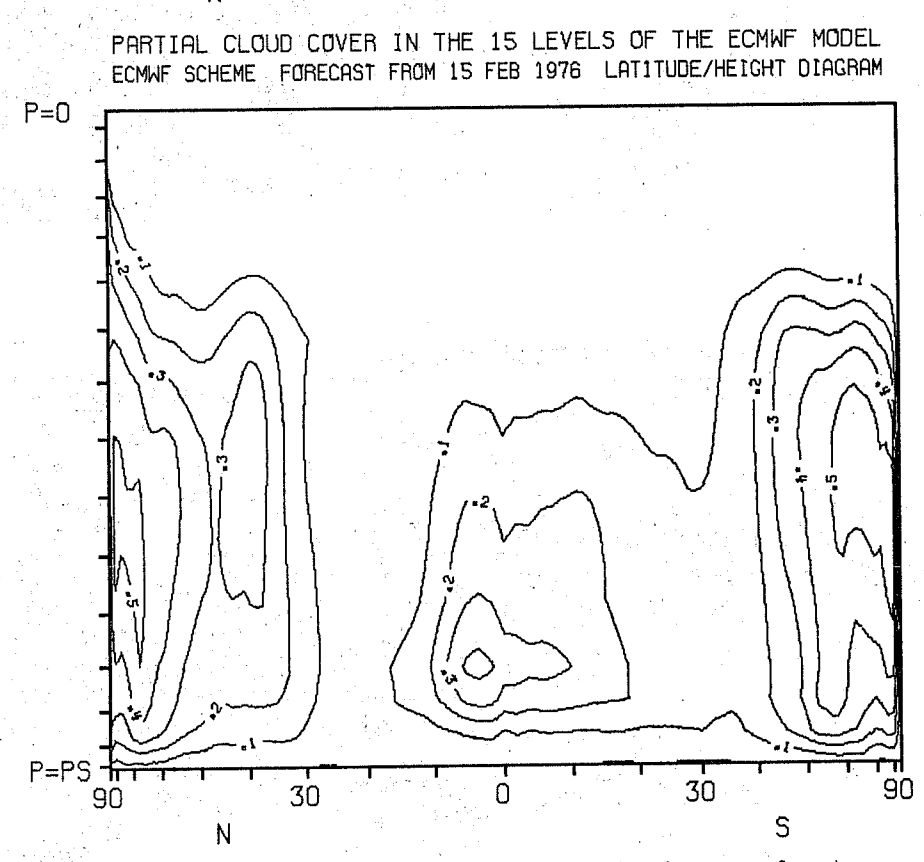

Fig. 4 Time and zonal average of cloud cover for two ten-day forecasts

Another way to look at the cloud field is to produce "pseudo satellite pictures" for the total cloud cover; an example is given in Fig. 5 where the field corresponding to a 5 day forecast is compared with the one of a 1 day forecast verifying at the same time. As a matter of "verification" the one day forecast is to be preferred to an analysis because at present our analysed humidity fields lack structure and as a consequence so do the derived cloud fields. One can see relatively good agreement and realistic looking patterns in the extratropical regions but a weakening of the cloudy features in the tropics and subtropics when going from the day 1 forecast to the day 5 forecast.

FORECAST D + 5 from 9/4/80 VERIFICATION 14/4/80

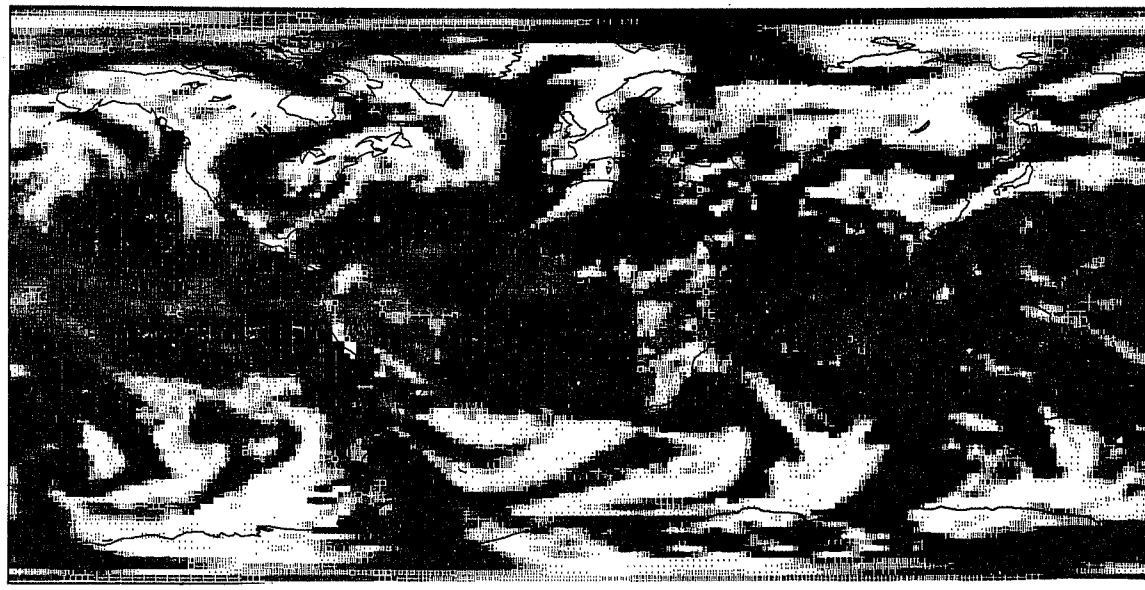

FORECAST D + 1 from 13/4/80 VERIFICATION 14/4/80

Fig. 5 Comparison of two "pseudo satellite pictures" for a 5-day forecast and a 1 day forecast verifying at the same time

As mentioned at the beginning of this section we shall now discuss the way in which the cloud field influences the radiative flux computations. The optical properties of cloud layers are computed from their liquid water content using data from Zdunkowski et al (1967). Both absorption/emission and scattering by all cloud layers are taken into account for the thermal spectrum as well as for the solar spectrum where the influence of the solar zenith angle is also considered. The details can be found in Geleyn and Hollingsworth (1979).

Special care has been given to the treatment of the cloud geometry for the case of more than one cloudy layer. Two principles guided our choice here: the equations should remain simple but the results should not depend on the position of the computation levels inside a given cloud ensemble. The solution adopted can be described rather simply for the parallel flux of solar radiation. The extension to diffuse fluxes and to thermal radiation albeit mathematically cumbersome is formally identical. Let us assume (Fig. 6A) that we know (from previous computations) both parallel solar fluxes S_c^1 and S_f^1 leaving the cloudy and cloud-free parts, respectively, of a layer 1 whose cloud cover is C_1. We shall assume a maximum overlap of the cloud parts of layers 1 and 2 and we then compute the fluxes S_c^2 and S^2 entering the cloudy and cloud free parts of 2 by linear combination of S_c^1 and S_f^1 :

$$\text{if } C_1 \leqslant C_2 \begin{cases} S_c^2 = S_c^1 + \dfrac{C_2 - C_1}{1 - C_1} S_f^1 \\ S_f^2 = \dfrac{1 - C_2}{1 - C_1} S_f^1 \end{cases}$$

$$\text{if } C_1 \geqslant C_2 \begin{cases} S_c^2 = \dfrac{C_2}{C_1} S_c^1 \\ S_f^2 = S_f^1 + \dfrac{C_1 - C_2}{C_1} S_c^1 \end{cases} \qquad (3)$$

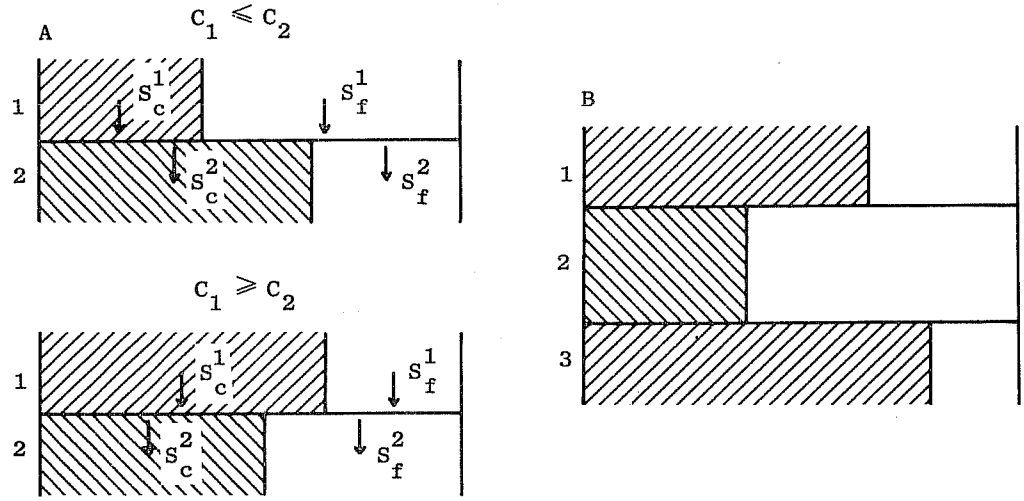

Fig. 6 Examples of cloud geometry for the illustration of the set of Equations 3.

The application of these principles on a cloud configuration such as the one of Fig. 6B indicates that the cloudy parts of layers 1 and 3 with a common overlap with the cloudy part of layer 2 are considered to be in the same vertical cloud while their other parts can be considered as having random positioning relative to one another.

This method is about twice as expensive (for the cloud treatment only) than the one in which one assumes full random positioning of cloudy areas. In the latter case transmissivities, reflectivities and emmisivities rather than fluxes, can be linearly combined but it appeared to us that the generality and consistency of our method was worth the expense. When we are considering the total cloud cover (Fig. 3, Fig. 5 and later) we refer to a value computed from the cloud covers at all model's layers. In fact it is one minus the proportion of the solar radiation at the top of the atmosphere that would reach the surface if clouds were totally opaque and cloud free areas totally transparent.

This description of the treatment in ECMWF's forecasting model of cloud/radiation interaction should be contrasted with the relatively crude way in which time evolution is taken into account. In our present system we have no diurnal cycle and solar radiative fluxes are computed for a mean of the positive values of the solar zenith angle and multiplied by the relative length of the day. These computations are carried out every twelve hours of integration at all model grid points using instantaneous values for temperature and humidity. One of our next goals is to introduce the diurnal cycle into the system.

4. ZONAL AND EDDY RADIATIVE FORCING

When trying to evaluate the errors of our zonally averaged radiative forcing, we came across an interesting and quite surprising result. We first integrated two ten day forecasts from a high predictability case (16.1.79). The first integration was a control "ECMWF" run, whilst in the second the radiative forcing, derived from Dopplick's (1972) data was used as a function of latitude and height only. In the "Dopplick" run therefore there was no eddy radiative forcing. The anomaly correlation coefficients, plotted as a function of time for the extra-tropical northern hemisphere troposphere for the zonal part of the flow as well as for the total flow, in Fig. 7, are as expected for this first comparison. If we disregard the dotted curve we see that the zonal part is predicted slightly better in the "Dopplick" run whilst the "ECMWF" run is best in terms of the total scores. One can then argue as follows.

The zonal forcing of the "Dopplick" experiment is closer to reality but the eddy variability of the interactive ECMWF scheme is important as well. One may ask, why not first compute as in the "ECMWF" run and then correct by the same margin all the radiative forcing values along a given latitude circle at a given height so that the zonal average is the one computed from the Dopplick data? The combination of the best features of both experiments should produce better results than either of the two individual experiments.

This was done in a third run, called thereafter "mixed" (dotted curve on Fig. 7). The result is as expected for the zonal part of the flow (the best of all three) but the total score is not as good as for the "ECMWF" experiment. The difference between "ECMWF" and "mixed" is the latter's destruction of consistency in the vertical and meridional radiative forcing. This surprising result shows how important is consistency in these two aspects. This can be contrasted with the good quality of the baroclinic meridional transport of heat in the interactive scheme that we mentioned in Section 2.

We tried to reproduce this result by carrying out tests ("Dopplick" and "mixed") on the same data sets as for CF and CA. The results were unfortunately inconclusive. In one case the "Dopplick" run was better than the ECMWF one, even for the total, and the reverse in the other case, even for the zonal part, so that the mixed cases cannot be meaningfully compared with the two other experiments. Even if not reproducible the result described above is a good indication that we must be careful with "obvious" improvements especially when we start using zonally averaged quantities.

These supplementary experiments were inconclusive, but, in the light of the sensitivity, to radiative forcing, of the ratio zonal to eddy kinetic energy as reported in this workshop by Cubasch, we felt it would be useful to use the same diagnostic for a comparison between "ECMWF" and "Dopplick". The result is shown in Fig. 8 which should also be compared with Fig. 6 of Cubasch. For the 10-day average both type of forecasts have similar "zonality". But we know that the "Dopplick" experiment has a zero radiative generation of eddy available potential energy (if one disregards the fact that the zonal forcing is in σ coordinated and not in pressure coordinates). Thus, if the influence of the different zonal forcings can be neglected, the "ECMWF" integration should also show a near zero generation term.

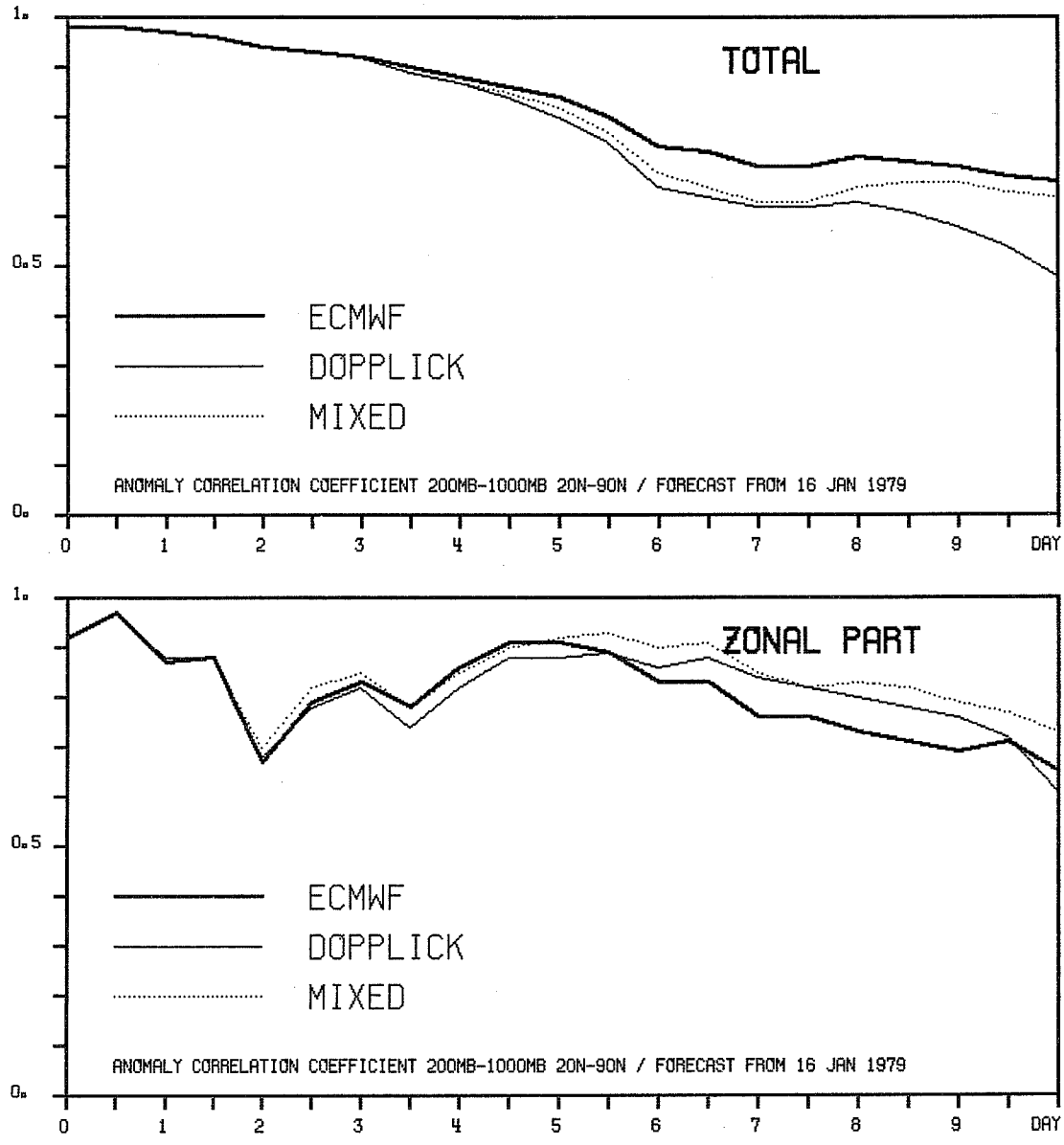

Fig. 7 Time evolution of anomaly correlation coefficients for the total flow and its zonal part in 3 experiments differing only by radiative forcing

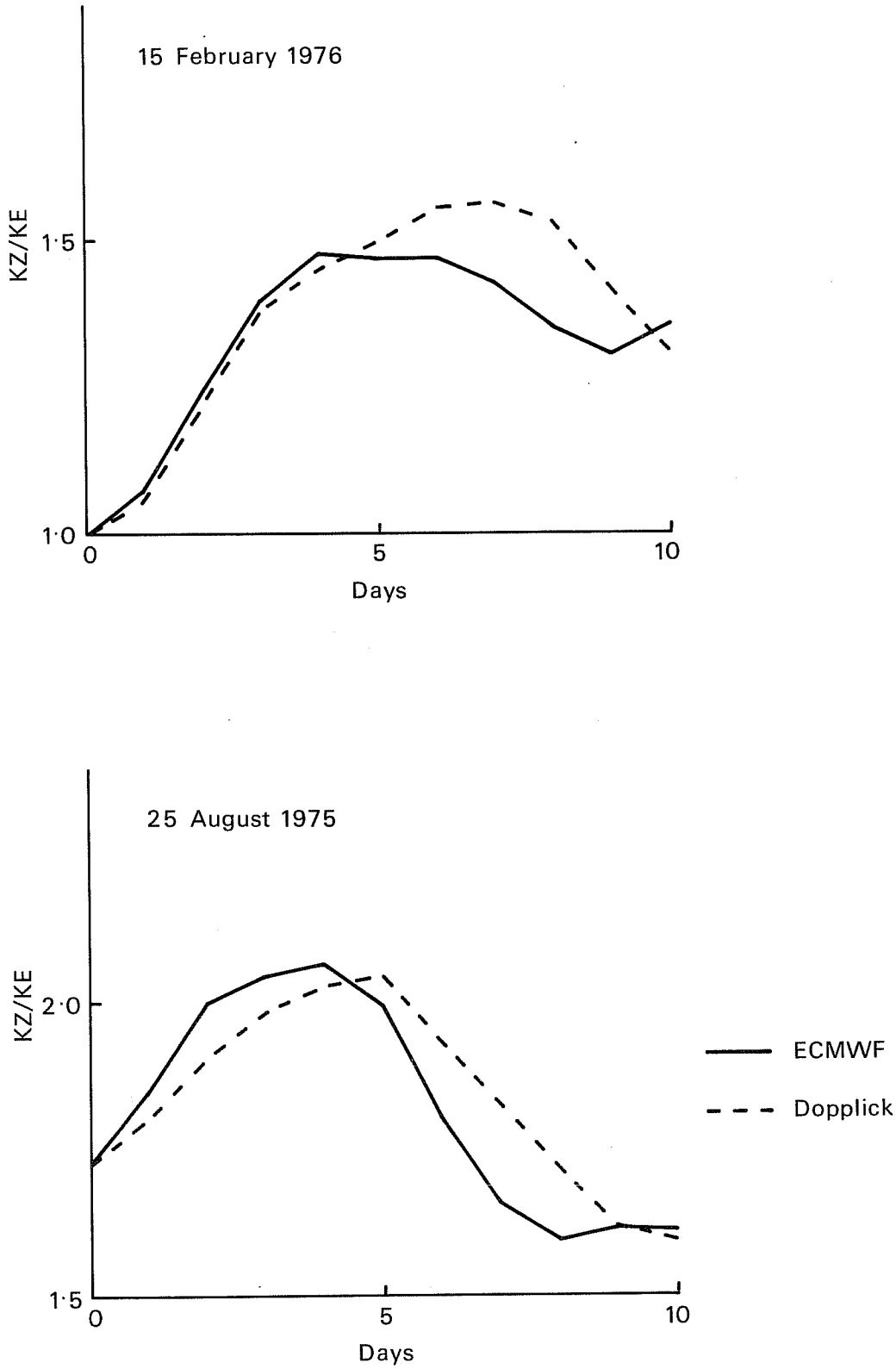

Fig. 8 Time evolution of the ratio zonal to eddy kinetic energy in two sets of two forecasts

We computed for experiments CF and CA the covariances of temperature and radiative heating on σ surfaces along latitude circles. This is not the radiative generation of eddy available potential energy but it is closely related to it. For mean tropospheric stability conditions $1^{\circ}K^2/day \simeq 1.4\ W/m^2$. When vertical averaging was performed it was either before the covariance computation (so called "whole atmosphere" computation) or after it (so called "sum over all levels" computation). The difference between both quantities indicate the degree of vertical inhomogeneity for these covariances. Results can be seen on Figs. 9, 10, 11 and 12 for the CF case.

For a better understanding of the results let us first start with a few remarks. The effect of temperature fluctuations taken alone is clearly one of damping (negative covariance) because Planck's emission law indicates that warmer parts of the atmosphere will have a stronger cooling than colder ones, all other things being equal. On the other hand the moisture and cloud fluctuations should have an opposite effect at least over a certain depth of the atmosphere. Clouds are generally indicating warm air and their relative radiative effect is a warming inside and underneath and a strong but localised cooling at the top. Thus we can expect generation (positive covariances) in the lower part of the atmosphere and dissipation in the higher. This is well illustrated in our model, see Figs. 11 and 12. We also expect the dissipation to be strong where temperature waves have large amplitudes and where clouds are present in both warm and cold parts of the wave (baroclinic activity regions), and the generation to be strong where clouds are an important heating factor for the atmosphere (tropics). This is also what is observed in our model, see Figs. 10 and 12. The extreme local maximum at $30^{\circ}N$ is probably irrelevant (caused by use of σ coordinate over the Himalayas) and must be disregarded. The fact that we seem to have a reasonable structure for this important energy term can perhaps explain the good quality of the kinetic energy of long waves in the control run when compared with the other runs in Section 2.

The time evolution, Fig. 9, (for CF and CA) shows that there is a "spin up" problem which has to do with the vertical structure of the moisture field but very little with its horizontal structure. As the analysis were not done with the ECMWF system, such a diagnosis should be repeated on one of our operational runs before more can be said. Otherwise, the fact that contrary to the scheme developed at the University of Köln (also shown on Fig. 9), generation and dissipation effects nearly compensate each other explains, at least partly, the difference in "zonality" apparent in Fig. 6 of Cubasch. The same is true for the comparison with the radiation scheme developed at GFDL since this scheme, where temperature is the only interactive non zonally averaged atmospheric parameter, can only have a negative covariance between temperature and radiative heating.

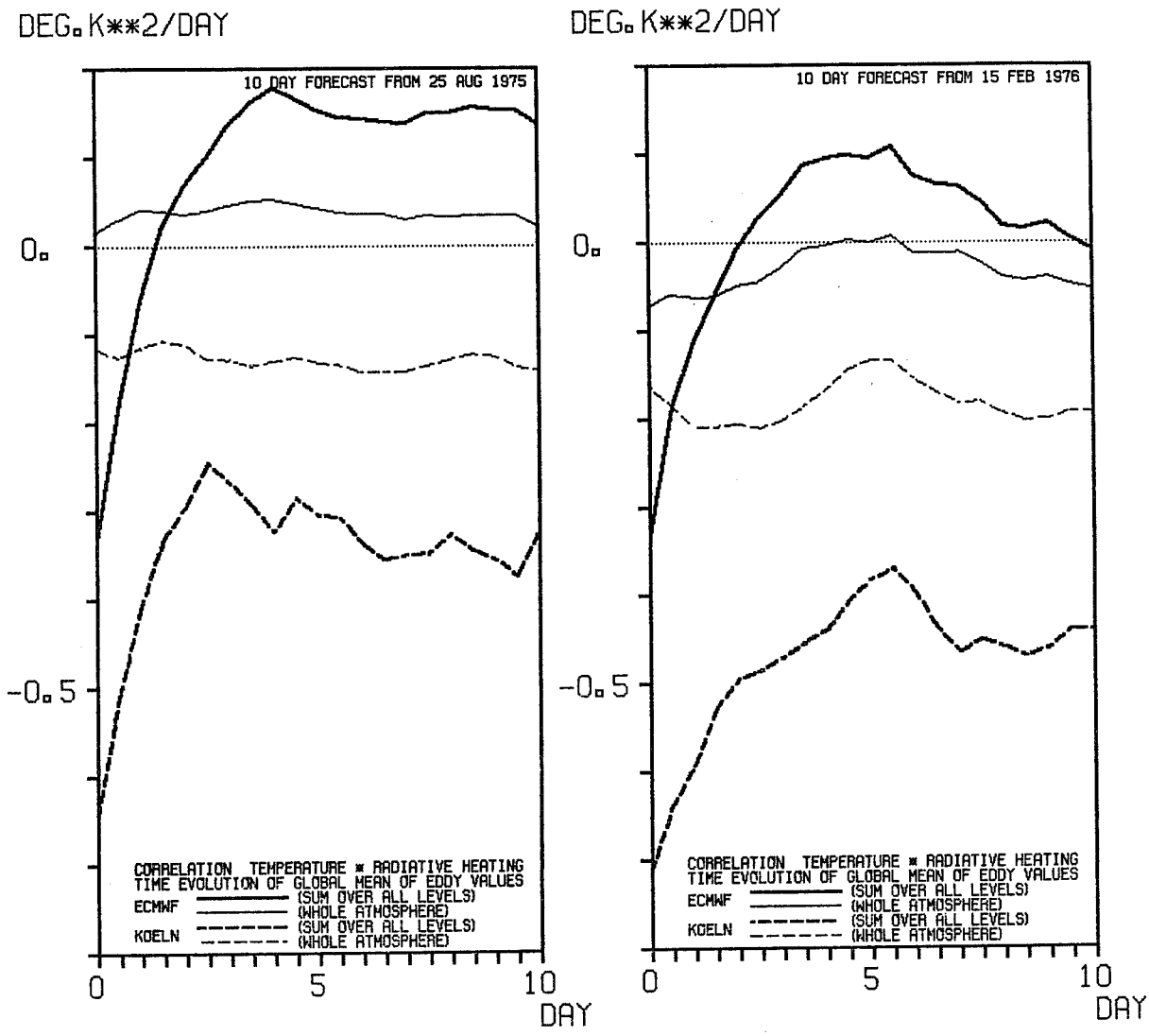

Fig. 9 Time evolution of the covariance between temperature and radiative heating on σ surfaces along latitude circles. Two cases. Two models.

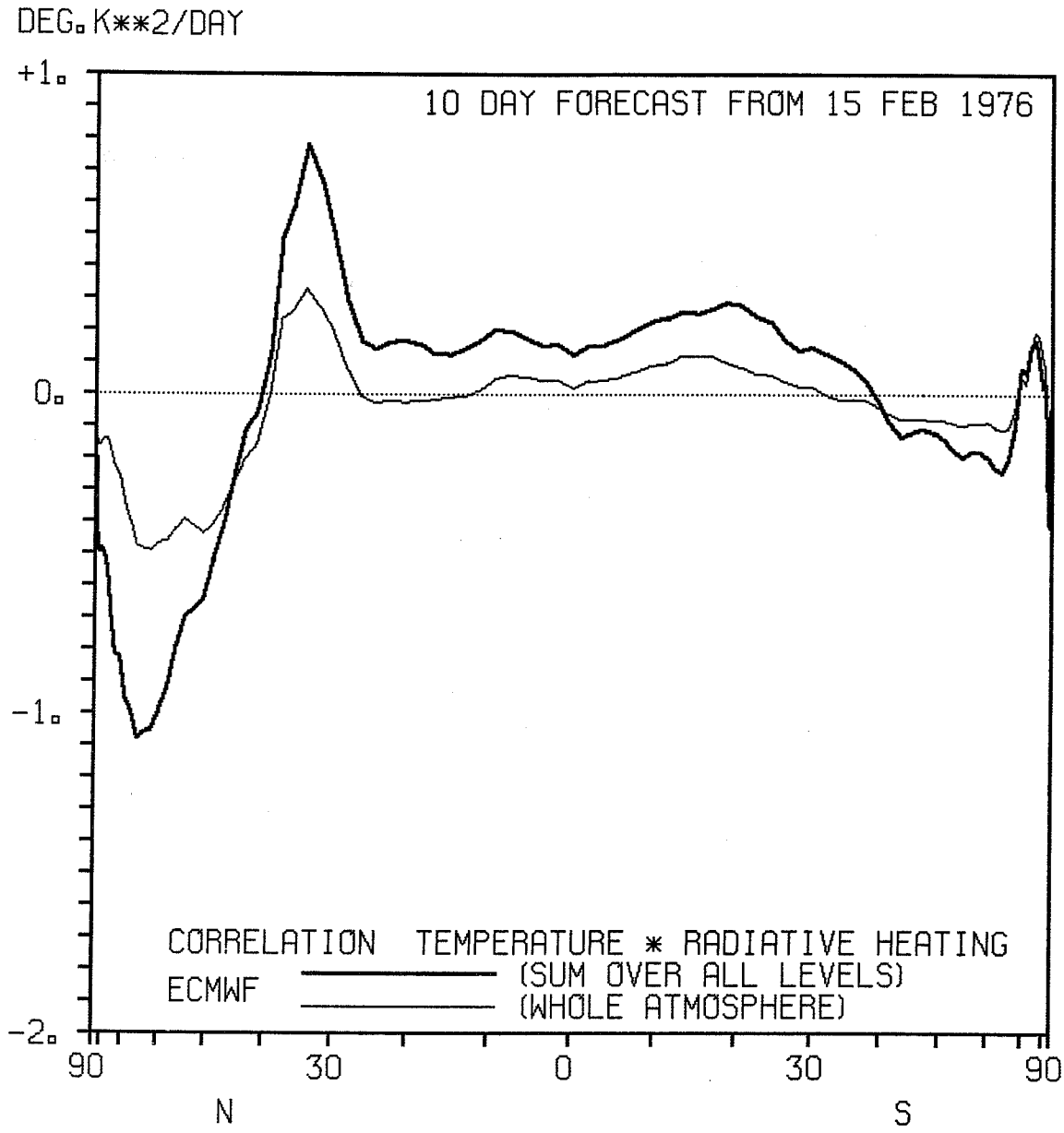

Fig. 10 Meridional structure of the covariance between temperature and radiative heating on σ surfaces along latititude circles. Average over one 10-day forecast.

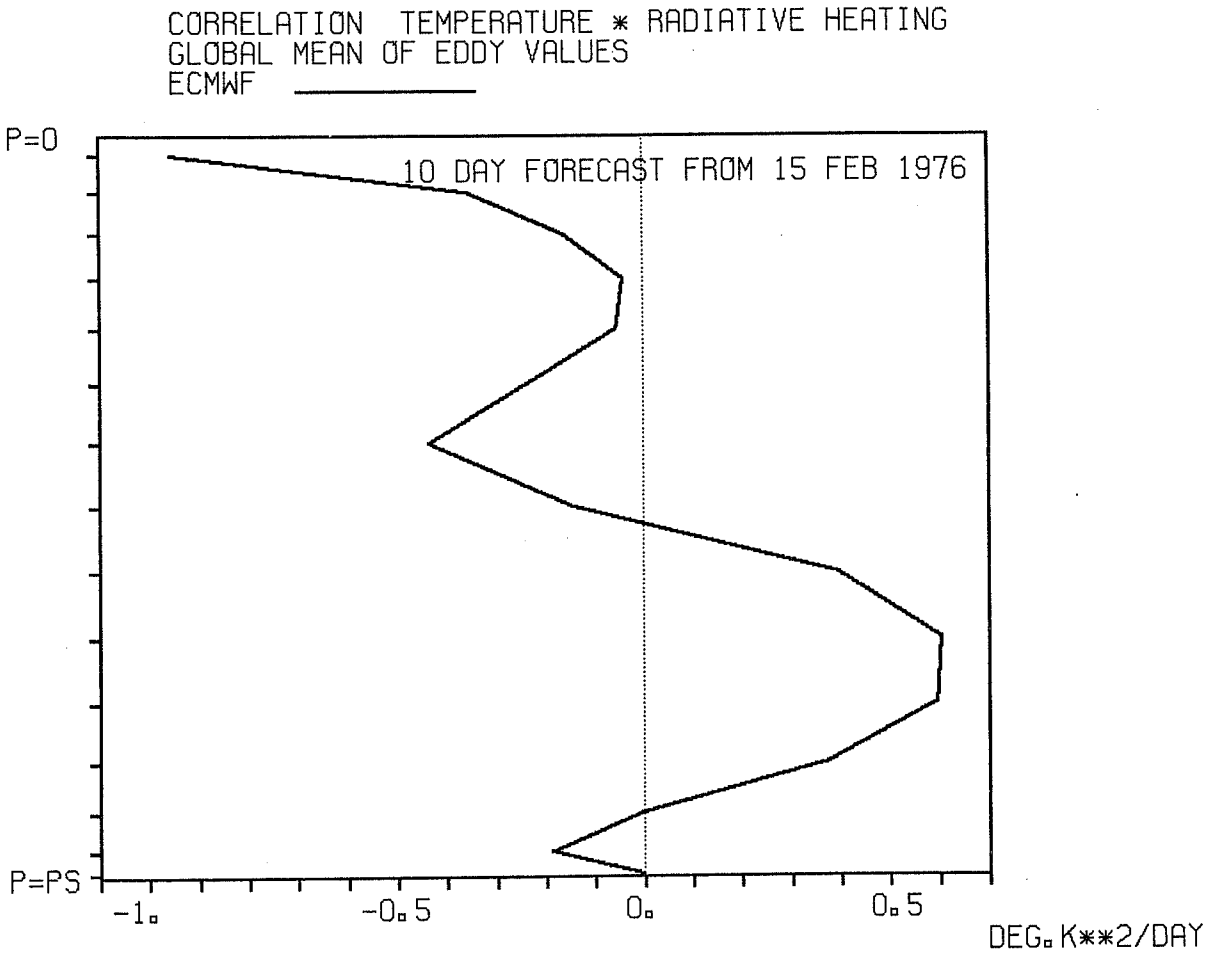

Fig. 11 Vertical structure of the covariance between temperature and radiative heating on σ surfaces along latitude circles. Average over one 10-day forecast

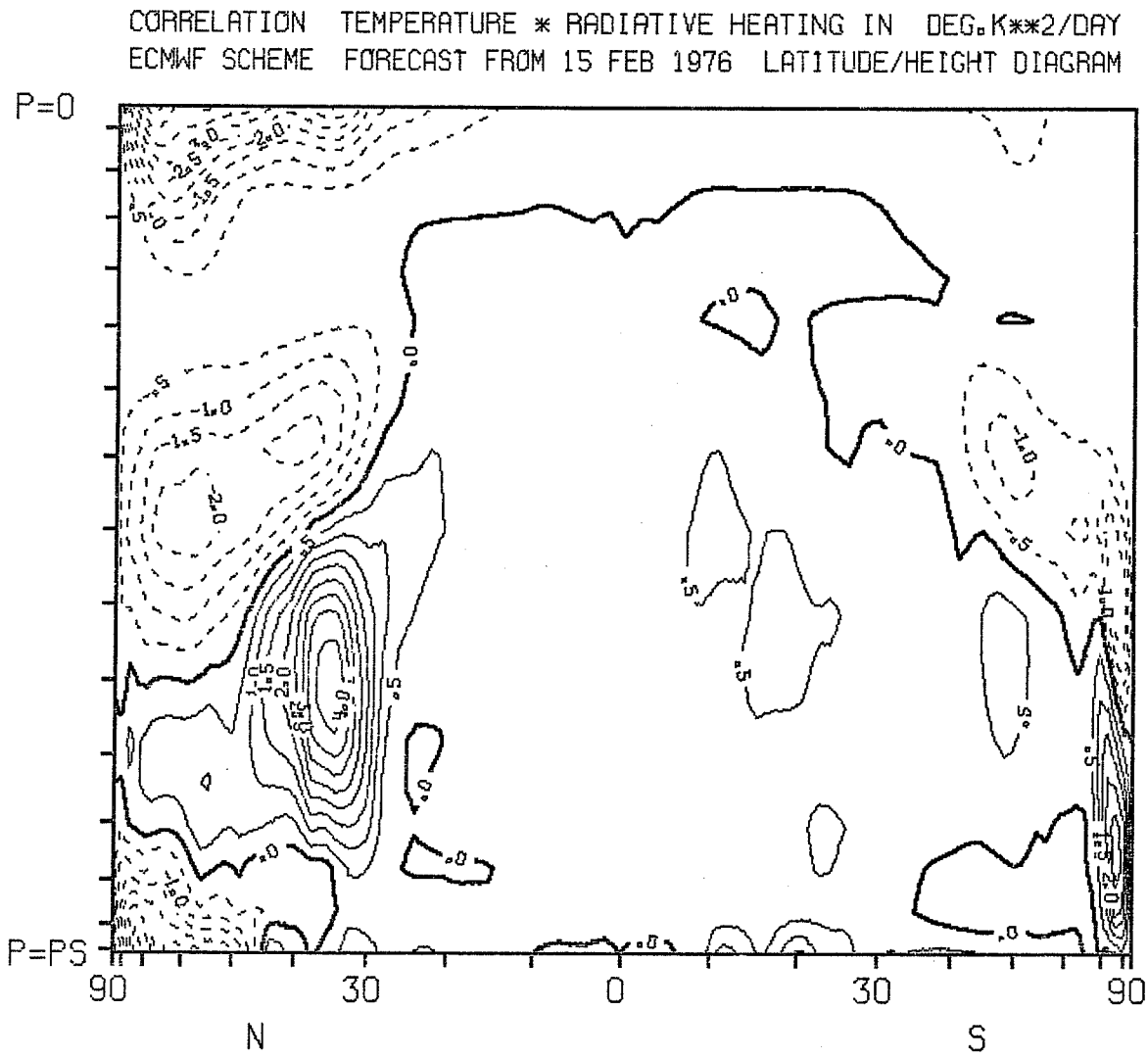

Fig. 12 Latitude height cross section of the covariance between temperature and radiative heating on σ surfaces along latitude circles. Average over one 10-day forecast.

The fact that the ratio zonal to eddy kinetic energy seems more reasonable in the ECMWF experiments is no proof that the radiative contribution is right: we could have the good result because of compensating errors, one in the radiation, one elsewhere. Nevertheless it might be considered as a positive indication. The only way to get the right result would be to have good surface radiation measurements over all the globe for a relatively short period where satellite data and good atmospheric analysis would also be available. Perhaps it will be possible with FGGE?

Until then, we must look at the vertical structure of our cloud forcing and compare global results with satellite measurements alone.

5. THE INFLUENCE OF CLOUDINESS ON HEATING RATES DURING ECMWF FORECASTS

To get a more relevant diagnosis of cloud dependent radiative cooling rates than that resulting from one-dimensional computations under idealised conditions, we decided to make such a diagnosis during the course of experiments CF and CA. We computed regression formula for the radiative heating rates in all model layers against the cloud covers in all model layers and against the total cloud cover. The results are shown for the CA case in Figs. 13, 14 and 15.

Fig. 13 shows a two-dimensional diagram of the "derivative" (the word "derivative" will from now on be used for "slope of the regression line") heating rate upon cloud cover. The horizontal axis represents the position of the cloud, of partial cover x, in the regression and the vertical axis the level of the heating rate, y, in the regression $y = ax + b$. The plot is therefore one of "a". The diagonal dotted line indicates where x and y are taken at the same level. Above the line means heating rate above the cloud, and below the line means heating rate underneath the cloud.

It should be noted that we do not see here the direct effect of a cloud on a layer, since the presence of a cloud somewhere is related to special temperature and humidity conditions in the adjacent layers. But these results are still very much as expected, cooling at the cloud top and aloft, warming underneath the cloud plus warming in the stratosphere for all clouds due to ozone's absorption of reflected solar radiation. The projection on the horizontal axis (Fig. 14) shows that the ECMWF system reproduces the well known result that low clouds have a strong cooling effect on the whole atmosphere while high tropospheric clouds have a slight warming effect. The pseudo projection on the other axis ("pseudo" since the total cloud cover is not the mean of all cloud covers) indicates (Fig. 15) that in our cloud distribution cloud/radiative interaction

has a cooling effect above 650 mb and a warming effect below, on average, over the whole earth. As previously these results cannot be verified directly against observation but they seem reasonable.

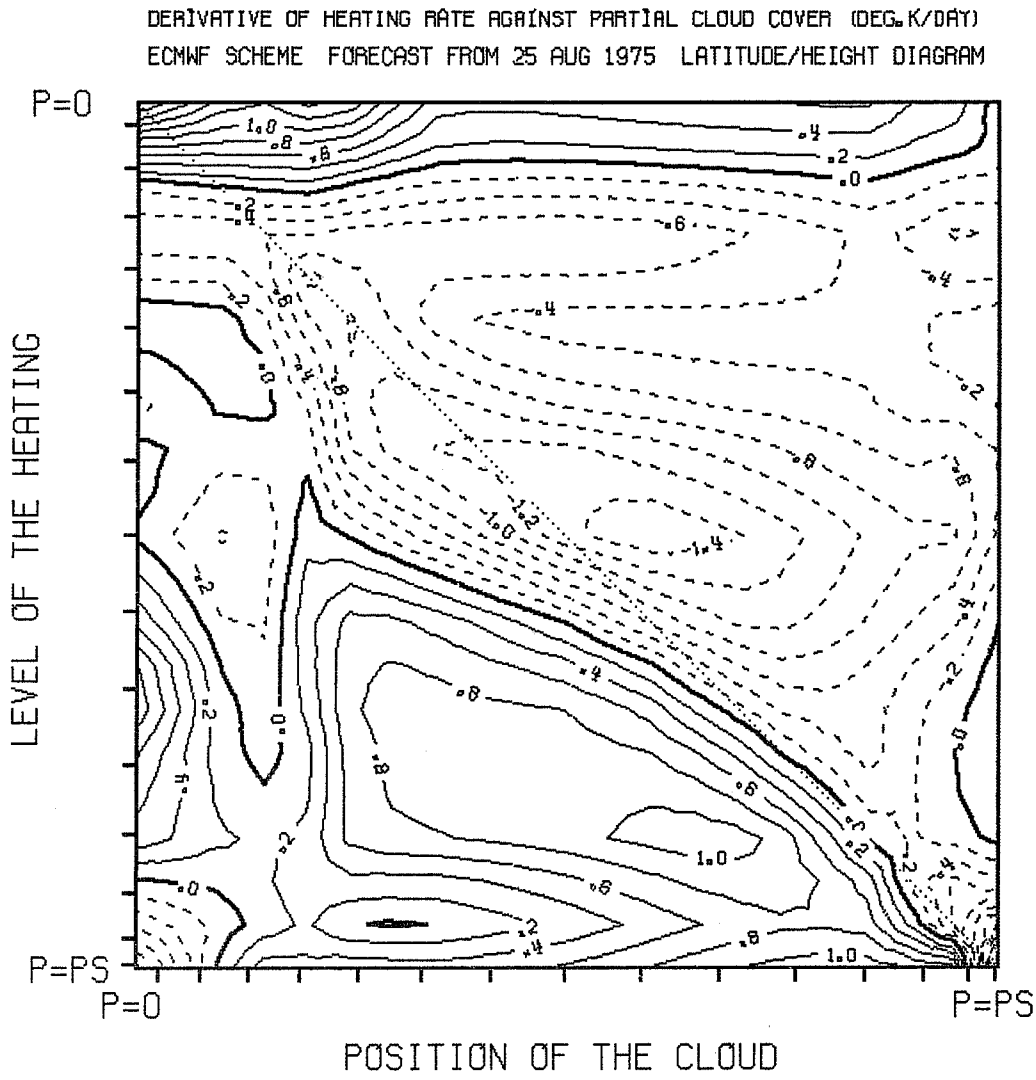

Fig. 13 Slope "a" of the regression curve y = ax+b (x = cloud cover at one model's layer; y = radiative heating at another (or the same) layer). Mean for the whole earth and a 10-day forecast in a 2 dimension diagram.

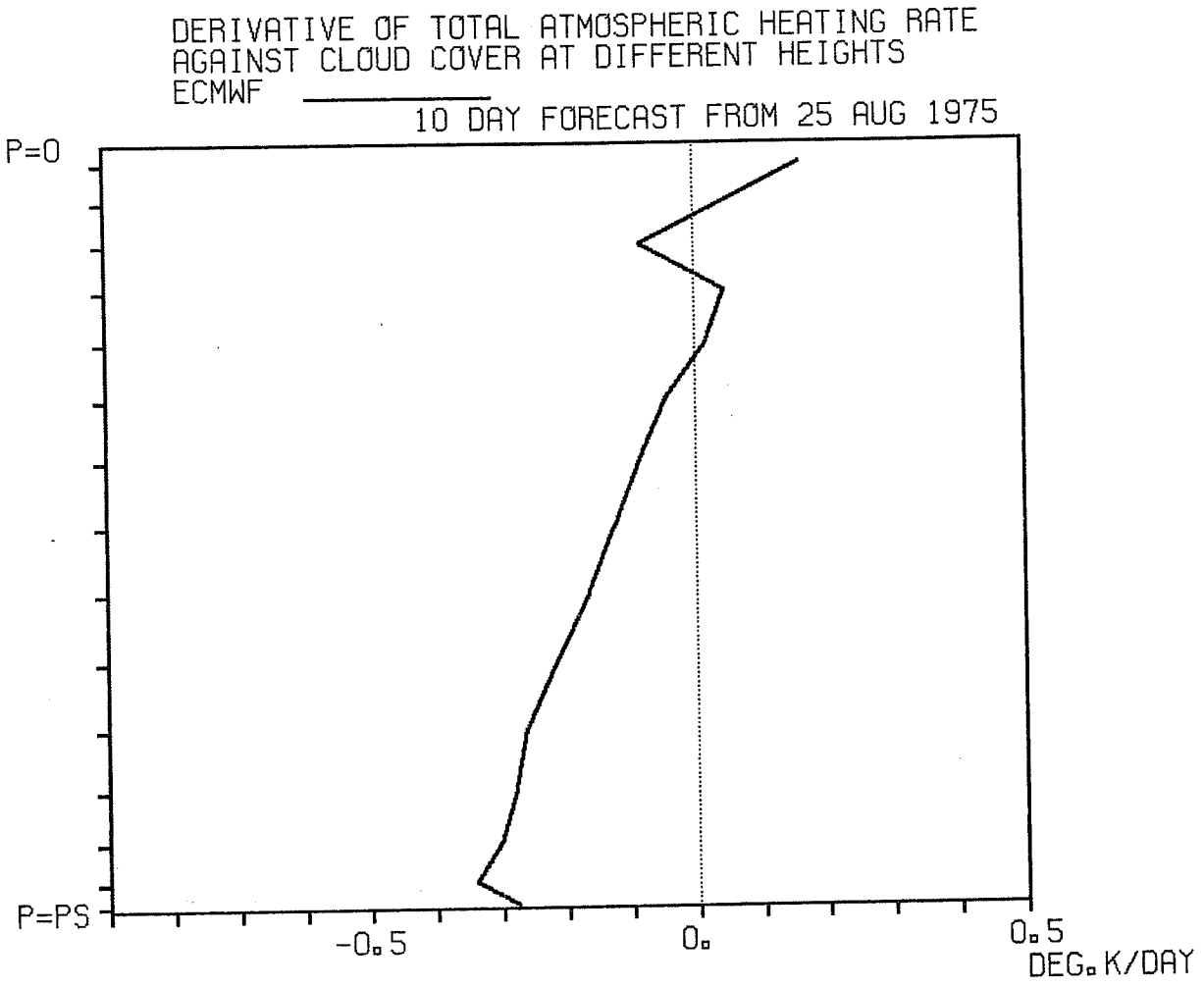

Fig. 14 Slope "a" of the regression curve y = ax+b (x = cloud cover at one model's layer; y = total atmospheric heating rate). Mean for the whole earth and a 10-day forecast versus position of the cloud.

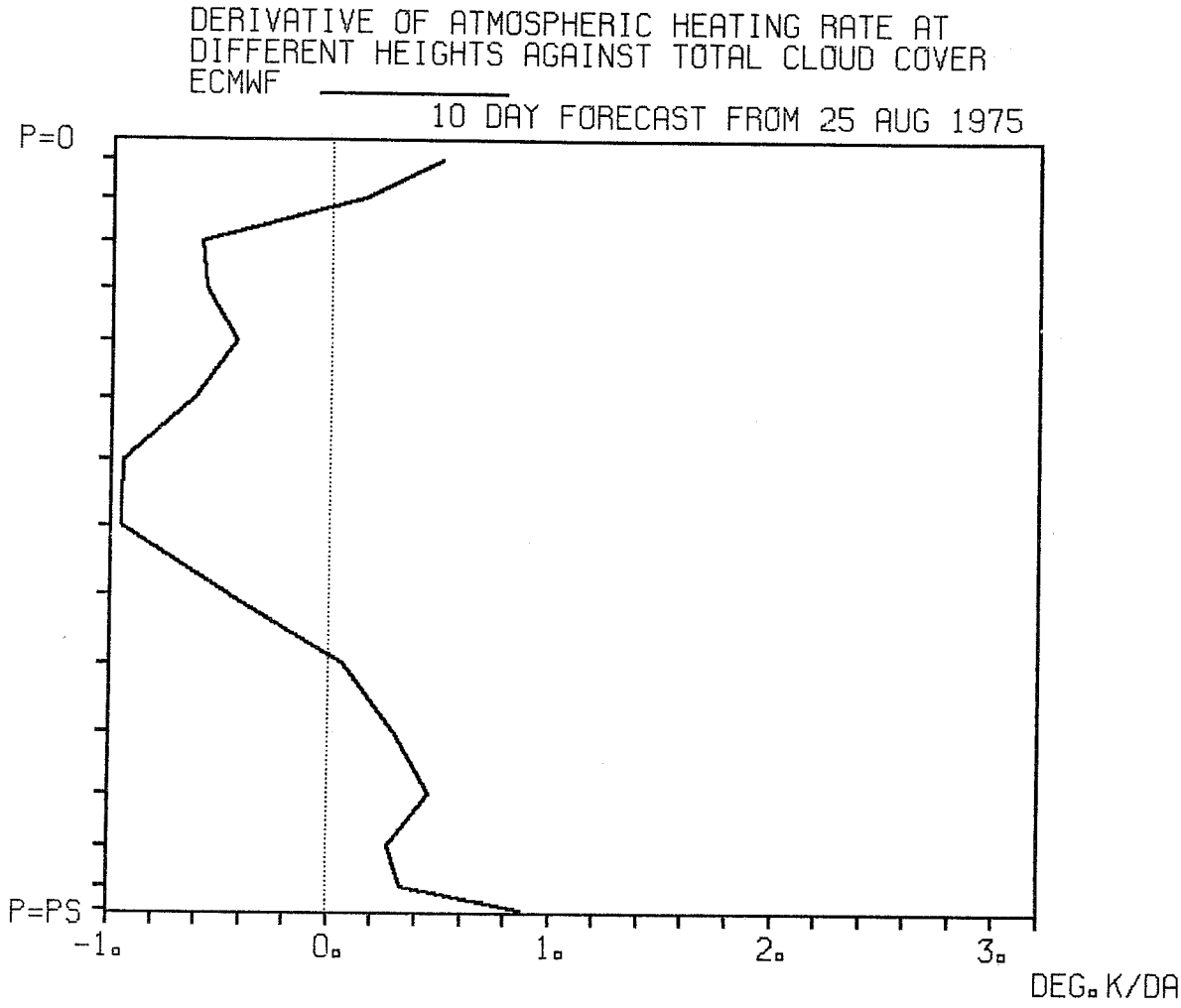

Fig. 15 Slope "a" of the regression curve y = ax+b (x = total cloud cover; y = radiative heating at one model's layer). Mean for the whole earth and a 10-day forecast versus height at which the heating is computed.

6. COMPARISON WITH SATELLITE DATA

Hense (1981) has shown in another presentation at this workshop that the temporal and zonally averaged fluxes from both Köln and ECMWF schemes compare quite well with NOAA measured fluxes for the experiments described in this workshop by Cubasch. These encouraging results lead us to attempt a more stringent test of the quality of the computed fluxes at the top of the atmosphere as compared with NOAA satellite measurements (Winston et al, 1979). We tried a regression analysis of the cloud albedo feedback. There are several ways of doing it (see for instance Hartmann and Short (1980)) but we decided to use the original form proposed by Ohring and Clapp (1980), that is to compute the "derivative" of the net downward radiative flux F at the top of the atmosphere against the planetary albedo A, and to use it as a measure of the compensation between the albedo effect and the greenhouse effect of clouds. If the regression has a negative slope the albedo effect is stronger if it is positive the greenhouse effect is stronger. Using the same NOAA data, but in monthly averages during a 3-year period and for small given geographic locations, Ohring and Clapp obtained negative slopes everywhere but in polar regions. Since our sample is short (2 times 10-day) we decided to make computations around latitude circles without time averaging. The variation of the surface albedo around these circles will make our results slightly less relevant (and different in any case from Ohring and Clapp's ones as we are not computing under the same conditions) but this should not affect the comparison model/satellite data since both types of data are treated in the same manner.

Table 3 summarizes the global results in terms of fluxes, regression formula and correlation coefficients for the regression and Figs. 16 and 17 show for CA and CF the meridional variations of the "derivative". Given the controversy in the recently published literature about even the sign of this quantity the results are very satisfactory.

Table 3. Comparison of global averages between NOAA observation and radiative computations with the "ECMWF" and "Köln" schemes for two 10-day forecasts run with the ECMWF global model for
S: downward solar flux at the top of the atmosphere (W/m^2)
T: upward thermal flux at the top of the atmosphere (W/m^2)
regression between F = S-T and A (planetary albedo)
c: correlation coefficient in the above regression

	NOAA	ECMWF	KÖLN
15.2.76	S=236 T=242 F=75 - 250.A c= 0.845	S=245 T=240 F=73 - 248.A c=0.812	S=227 T=240 F=63 - 218.A c=0.821
25.8.75	S=230 T=224 F=84 - 253.A c=0.495	S=243 T=252 F=56 - 245.A c=0.858	S=229 T=251 F=39 - 197.A c=0.837

The smaller values for the "derivatives" with the Köln scheme can entirely be explained by the higher albedo values (cf. S in Table 3) themselves mainly due to a different treatment of the same cloud field (random overlapping instead of the system explained in Section 3 for which the tuning was done in the ECMWF version).

In Figs. 16 and 17 as in Fig. 3 our performance in the tropics exhibits a different behaviour from the rest and the correction of the tropical error mentioned in Section 3 would probably decrease the quality of this simulation.

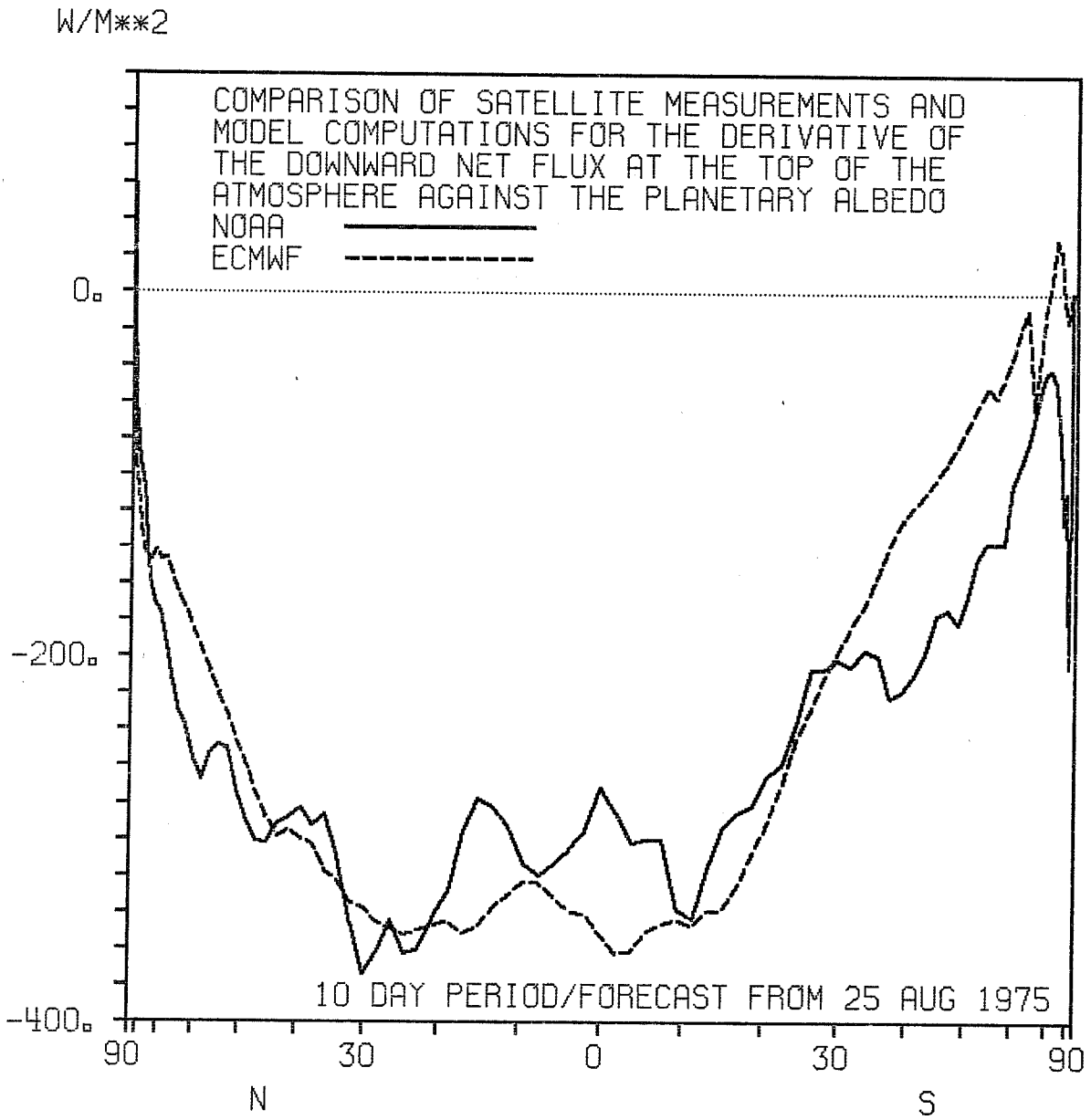

Fig. 16 Comparison of observed and computed differences between albedo effect and greenhouse effect of cloudiness for the 10-day period starting 25.8.75 plotted against latitude.

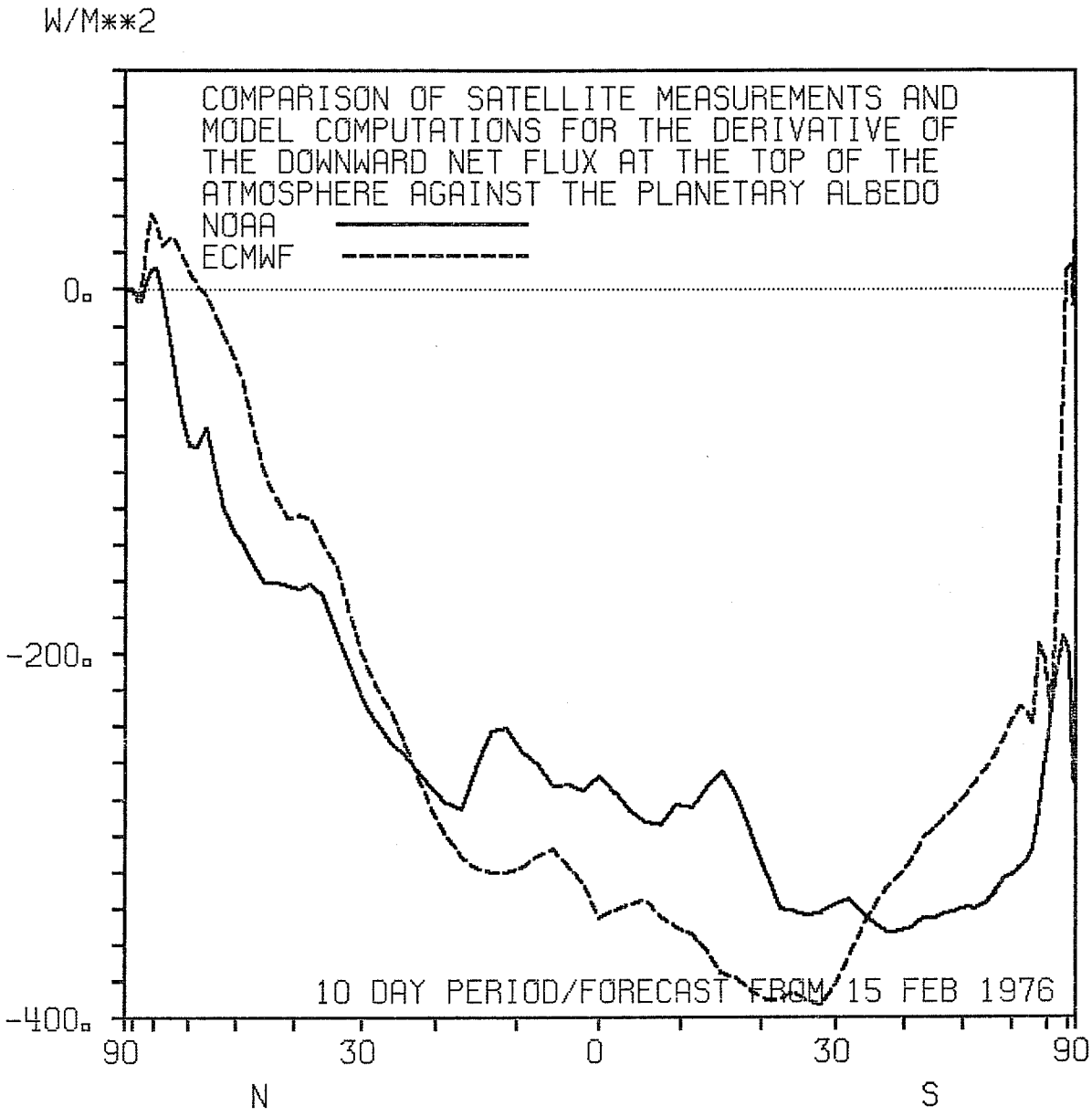

Fig. 17 Comparison of observed and computed differences between albedo effect and greenhouse effect of cloudiness for the 10-day period starting 15.2.76 plotted against latitude.

7. CONCLUSIONS

Despite three weaknesses (stratospheric cooling, insufficient boundary layer cooling and too low tropical clouds) the present ECMWF system for the parameterization of radiation and cloud/radiation interaction seems able, mainly because of its interactive character, to simulate rather realistically some aspects of real atmospheric phenomenon.

It would be interesting to compare the results reported here (in Sect. 4, 5, 6 essentially) with the ones of several different radiation schemes running either under the same conditions or with other global models. The comparison with the Köln scheme was very fruitful for both groups of people concerned and we hope that this type of work can be pursued and extended in the future.

References

Cox, S. and Griffith, K.T., 1979 Estimate of radiative divergences during Phase III of the GARP-Atlantic Tropical Experiment. J.Atmos.Sci., 36, 586-601.

Cubasch, U., 1981 Comparison of the influence of different radiation parameterizations on 10 day forecasts. ECMWF Workshop on "Radiation and Cloud-Radiation interaction in numerical modelling"

Dopplick, T.G., 1972 Radiative heating of the global atmosphere. J.Atm.Sci., 29, 1278-1294.

Geleyn, J.-F. and Hollingsworth, A., 1979 An economical analytical method for the computation of the interaction between scattering and line absorption of radiation. Beitr.Phys.Atmosph., 52, 1-16.

Hartmann, D.L. and Short, D.A., 1980 On the use of Earth Radiation Budget statistics for studies of clouds and climate. J.Atm.Sci., 37, 1233-1250.

Hense, A., 1981 Cloud Radiation Parameterization Schemes. ECMWF workshop on "Radiation and Cloud-Radiation interaction in numerical modelling".

Hoyt, D.V., 1976 The radiation and energy budgets of the earth using both ground based and satellite-derived values of total cloud cover NOAA Technical Report ERL 362-ARL4

London, J., 1952 The distribution of radiational temperature change in the Northern Hemisphere during March. J.Meteorol., 9, 145, 151.

Ohring, G. and Clapp, P., 1980 The effect of changes in cloud amount on the net radiation at the top of the atmosphere. J.Atm.Sci., 37, 447-454.

Winston, J.S., Gruber, A., Gray, T.I., Varnadore, M.S., Earnest, C.L. and Manello, L.P., 1979 Earth Atmosphere Radiation Budget derived from NOAA satellite data June 1974 - February 1978 NOAA S/T 79-187, Vol. 1 and 2.

Zdunkowski, W.G., Korb, G.J. and Niessen, B.C., 1967 Prediction and maintenance of radiation fog. US Army Electronics Command Report, Contr. DAAB 07-67. C-0049.